 Bull. Chem. Soc. Jpn., **74**, 1605–1610 (2001)

Optical–Optical Double Resonance Spectroscopy of I_2 through the Parity Mixed Valence States

Takashi Ishiwata,* Takashi Yotsumoto, and Satoshi Motohiro

Faculty of Information Sciences, Hiroshima City University, Ozukahigashi, Hiroshima 731-3194

(Received March 16, 2001)

We used the perturbation-facilitated optical–optical double resonance technique to access the *ungerade* ion-pair states of I_2 using the (1 + 1) photo-excitation sequence through the $B^3\Pi(0_u^+)$–$c1_g$ parity mixing states. By analyzing the second step of the double resonance to the $F0_u^+(^3P_0)$, $\gamma 1_u(^3P_2)$, and $H1_u(^3P_1)$ states, the *g*–*u* coupling schemes were elucidated in the intermediate $B^3\Pi(0_u^+)$–$c1_g$ state. We were also able to populate the $\delta 2_u(^3P_2)$ state through the *g*–*u* mixing state, and to improve its molecular constants. The interference effect between the parallel $\gamma 1_u(^3P_2)$–$c1_g$ and perpendicular $\delta 2_u(^3P_2)$–$c1_g$ transitions was used to derive the ratio of their electronic transition moments, $(\mu_\parallel^e/\mu_\perp^e) \sim 5.5$.

Homonuclear diatomic molecules have the inversion symmetry (*i*). The electronic states are usually labeled as *gerade* or *ungerade* in respect to the symmetry against the operation *i*, depending on whether the electronic wavefunctions are even or odd, respectively.[1] This symmetrical property does not break even by non-Born–Oppenheimer terms. The *g*–*u* symmetry breaking only occurs through the hyperfine coupling in a non-zero-nuclear-spin diatomic molecule.[2] Pique et al. gave the direct evidence of this phenomenon in the visible absorption spectrum of I_2 and identified this as occurring between the rovibronic levels of the $B^3\Pi(0_u^+)$ and $c1_g$ states near the dissociation limit.[3,4]

Above the valence states, the iodine molecule has 20 ion-pair states correlating with I^+ (^{3}P, ^{1}D, ^{1}S) + $I^-(^1S)$ at the dissociation limit.[5] They consist of the same number of the *g*- and *u*-states as described in Hund's case c. We usually applied optical–optical double resonance spectroscopy to observe these states in the (1 + 1) photo-excitation scheme for the *g*-states and that in the (1 + 2) scheme for the *u*-states in view of the parity selection rules for the optical transitions. Either the $A^3\Pi(1_u)$ or $B^3\Pi(0_u^+)$ valence state is used as an intermediate in view of the $\Delta\Omega = 0$ propensity rule for the valence state to ion-pair state transitions having the charge transfer property along the internuclear axis.[6–9]

In addition to these excitation schemes used for the systematic approach, we are able to access the ion-pair states by perturbation-facilitated optical–optical double resonance through the *g*–*u* mixed levels. Danyluk and King carried out the double resonance experiments through the high vibrational levels of the $B^3\Pi(0_u^+)$ state using the (1 + 1) photo-excitation scheme.[10] They observed five ion-pair states in the 40000 cm^{-1} region above the ground state and named them as α, β, γ, δ, and ε in order of increasing frequency of the first member of vibrational progressions. The six states (0_g^+, 1_g, 2_g, 0_u^+, 1_u, and 2_u) correlating with $I^+(^3P_2)$ + $I^-(^1S)$ are now known to lie in this energy region. All available evidence shows that α, β, and ε correspond to the transitions to the $2_g(^3P_2)$, $1_g(^3P_2)$, and $0_g^+(^3P_2)$ states, respectively (5). The remaining two, γ and δ, are recently identified as the $1_u(^3P_2)$ and $2_u(^3P_2)$ states, respectively.[11,12] Therefore it is now recognized that the pioneering work of Danyluk and King involves the double resonance excitation to the symmetry-forbidden destination states by choosing a coupled intermediate state of mixed electronic parity. Jewsbury et al. recently showed that this mixing occurs between the resonant $B^3\Pi(0_u^+)$ and $c1_g$ states and applied this technique to locate a new ion-pair state, $H1_u(^3P_1)$.[11]

The purpose of this paper is to report the results of perturbation-facilitated optical–optical double resonance spectroscopy of I_2 through the parity mixed states. We first elucidate the *g*–*u* perturbation in the $B^3\Pi(0_u^+)$ state while focusing attention on the coupling scheme between the $B^3\Pi(0_u^+)$ and $c1_g$ valence states. The selection rule of hyperfine coupling is $\Delta \boldsymbol{F}$ (= $\boldsymbol{I}$ + $\boldsymbol{J}$) = 0, which allows a change of rotational angular momentum between the coupled rotational levels of the $B^3\Pi(0_u^+)$ and $c1_g$ states. We pump the molecules to the $B^3\Pi(0_u^+)$–$c1_g$ mixing state and examine the second step of the double resonance to the well-characterized $F0_u^+(^3P_0)$, $\gamma 1_u(^3P_2)$, and $H1_u(^3P_1)$ states in view of the optical selection rules and by energy level analysis.[8,12] We define the coupling schemes between the resonant $B^3\Pi(0_u^+)$ and $c1_g$ states in several rovibronic levels, which enable us to carry out the double resonance experiments on unknown ion-pair states. Secondly, we demonstrate the ability of this technique by probing the $\delta 2_u(^3P_2)$ state in the (1 + 1) photo-excitation sequence. The previous experiments allowed us to observe the $\delta 2_u(^3P_2)$ state only by the intensity borrowing through the mixing with the $\gamma 1_u(^3P_2)$ state.[12] Even though the $\delta 2_u(^3P_2)$–$c1_g$ does not obey the $\Delta\Omega = 0$ propensity rule, the $\delta 2_u(^3P_2)$ state is detected directly and the molecular constants of the $\delta 2_u(^3P_2)$ state can be greatly refined. We find the interference effects on the intensities of the P and R branches in the $\delta 2_u(^3P_2)$–$c1_g$ transition and derive the ratio of the electronic transition moments between the $\gamma 1_u(^3P_2)$–$c1_g$ and $\delta 2_u(^3P_2)$–$c1_g$ systems.

Experimental

The experimental setup used in this study is similar to that de-

scribed previously.[9] Briefly, we used two tunable lasers simultaneously excited by a Nd:YAG laser. The outputs of the lasers were aligned coaxially and passed along the axis of an absorption cell containing iodine. The pump laser excited the visible $B^3\Pi(0_u^+)$–$X^1\Sigma_g^+$ absorption line for state selection at the fixed frequency ($h\nu_1$). The probe laser frequency ($h\nu_2$) was scanned to excite the molecules subsequently to the ion-pair states in the (1 + 1) photo-excitation sequence from the intermediate state. The double resonance transition was detected by an emission of the ion-pair state down to the valence state through a monochromator. Photomultiplier signals were integrated by a boxcar.

There was a 5-ns delay between two laser pulses of 7-ns duration. The sample pressure was about 0.2 Torr (1 Torr = 133.322 Pa), which was low enough to exclude the collisional relaxation in the intermediate state. Coumarine 307 was used as the pump dye to excite the $B^3\Pi(0_u^+)$–$X^1\Sigma_g^+$ absorption band. Coumarine 2 and Coumarine 47 were used as the probe dyes to access the $\gamma 1_u(^3P_2)$ and $\delta 2_u(^3P_2)$ states, while Pyridine 1 and Styryl 7 were used for probing the $F0_u^+(^3P_0)$ and $H1_u(^3P_1)$ states by their frequency doubled outputs, respectively. The bandwidth of the tunable lasers was 0.02 cm^{-1} in the case of operating with étalon. The laser wavelength was then calibrated by reference to the absorption spectrum of I_2 in the infrared and visible regions down to 500 nm, and that of Te_2 beyond this limit.[13–15]

Results and Discussion

1 Parity Mixing between the $B^3\Pi(0_u^+)$ and $c1_g$ States. Figure 1 shows two examples of the double resonance spectra observed through the $B^3\Pi(0_u^+)$–$c1_g$ mixing states. We tuned the pump laser frequency to the (59-0) band of the $B^3\Pi(0_u^+)$–$X^1\Sigma_g^+$ system where the parity mixing with the $c1_g$ $v = 14$ state was identified previously.[11] The pump laser excites the (59-0)P_{23} and R_{24} transitions in spectrum (a) and the (59-0)P_6 and R_7 transitions in spectrum (b). The probe laser was scanned in the 367.2–365 nm range by collecting the emission at 270 nm.

Two vibrational progressions in these spectra are assigned to the transitions to the $E0_g^+(^3P_2)$ and $F0_u^+(^3P_0)$ states from their known spectroscopic constants, as shown in Fig. 1.[6,8] The first step of excitation to intermediate state, in which the $B^3\Pi(0_u^+)$–$c1_g$ mixing occurs, is executed through its $B^3\Pi(0_u^+)$–$X^1\Sigma_g^+$ property. In the second step, the molecules are excited to either the $E0_g^+(^3P_2)$ or $F0_u^+(^3P_0)$ state from the intermediate state, depending on the probe laser wavelength by its $B^3\Pi(0_u^+)$ and $c1_g$ double-faced character:

$$\begin{array}{ccc} E0_g^+(^3P_2) & & F0_u^+(^3P_0) \\ \uparrow h\nu_2 & & \uparrow h\nu_{2'} \\ B^3\Pi(0_u^+) & \sim & c1_g \\ \uparrow h\nu_1 & & \\ X^1\Sigma_g^+. & & \end{array} \quad (1)$$

The progression terminating on the $v = 65$–67 levels of the $E0_g^+(^3P_2)$ state consists of two sets of the P and R doublets. The excitation to the $E0_g^+(^3P_2)$ state occurs from two rotational levels of the $B^3\Pi(0_u^+)$ state excited by the pump laser according to the $\Delta J = \pm 1$ rotational selection rule for the $E0_g^+(^3P_2)$–$B^3\Pi(0_u^+)$ transition. On the other hand, it should be noticed that the transition to the $F0_u^+(^3P_0)$ state occurs in a single Q branch in spectrum (a) and in the P and R branches in spectrum (b) for several reasons.

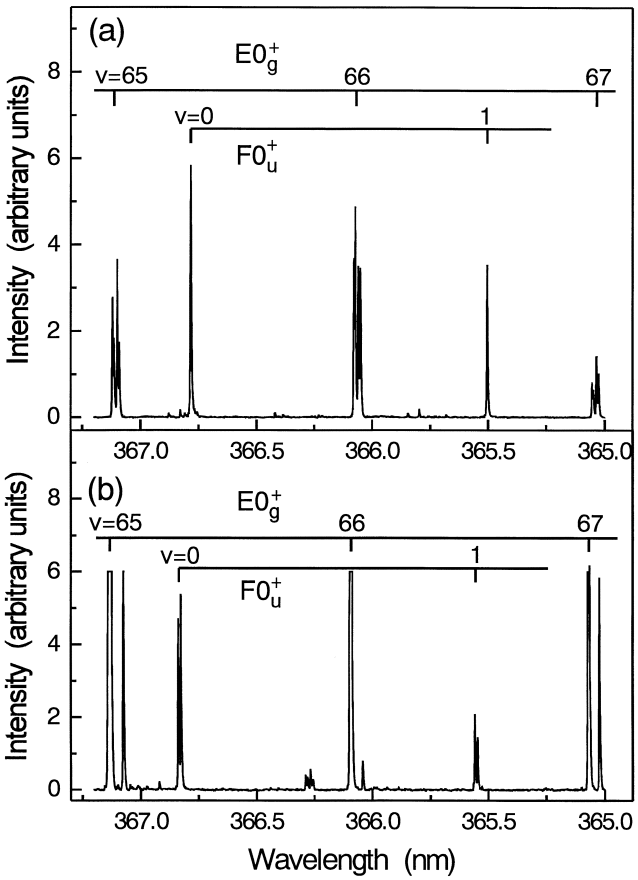

Fig. 1. Double resonance spectra observed (a) through the (59-0)P_{23} and R_{24} transitions and (b) through (59-0)P_6 and R_7 transitions of the $B^3\Pi(0_u^+)$–$X^1\Sigma_g^+$ system. Emission collected at 270 nm.

(i) Jewsbury et al. reported the degree of hyperfine coupling between the B($v = 59$, J_B) and c($v = 14$, J_c) as a function of J_B, where J_B and J_c denote the rotational quantum numbers of the $B^3\Pi(0_u^+)$ and $c1_g$ states in the parity mixing state, respectively.[11] They showed that the *g*–*u* coupling was quite sensitive on J_B due to a small value of the effective coupling term, $H_{12} \sim 0.01$ cm^{-1} and that there was a sharp peak at $J_B = 22$ with a very minor peak at $J_B = 8$. Therefore, the pump laser populates two rotational states, $J_B = 22$ and 25 in spectrum (a), of which only the first is strongly coupled to the $c1_g$ state to access the $F0_u^+(^3P_0)$ state. One can easily confirm that the same Q branch occurs in the double resonance spectrum when we tuned the pump laser to the (59-0)R_{21} branch. Following the same procedure, we find that the double resonance transitions to the $F0_u^+(^3P_0)$ occur only by exciting the molecules to the $J_B = 8$ level of the $B^3\Pi(0_u^+)$ state in spectrum (b).

(ii) In I_2, the coupling of nuclear spin with the electronic angular momentum can mix rovibronic states of opposite electronic parity.[2] Each rotational state, though to a small extent, splits into the hyperfine components defined by the quantum number $\boldsymbol{F} = \boldsymbol{I} + \boldsymbol{J}$ due to the coupling of the rotational and angular momenta. The hyperfine interaction combines the states of $\Delta \boldsymbol{F} = 0$, which allows a change of the rotational quantum numbers $\boldsymbol{J}$ between the $B^3\Pi(0_u^+)$ and $c1_g$ states.

(iii) The $c1_g$ state is degenerate and is composed of e and f sublevels. From the parity property in the mixing intermediate states, we expect two types of patterns in the rotational transitions in the second step of the double resonance transition to the $F0_u^+(^3P_0)$ state, depending on the coupling scheme.

For example, as shown in case (b) of Fig. 2 for even J levels of the $B^3\Pi(0_u^+)$ state, if one first supposes that the hyperfine coupling occurs between the states of $\Delta J = J_c - J_B = 1$, the $B^3\Pi(0_u^+)$ state is combined with the f sublevel of the $c1_g$ state because of the conservation of parity property of two rotational states ($+ \leftrightarrow +$ and $- \leftrightarrow -$) in the perturbation. The rotational selection rules for the perpendicular $F0_u^+(^3P_0)$–$c1_g$ transition are $\Delta J = 0$ and ± 1. However, the P and R branch transitions are missing from the intermediate state and only a single Q branch is expected in the $F0_u^+(^3P_0)$–$c1_g$ transition due to the parity selection rule of optical transition ($+ \leftrightarrow -$). And it is easy to recognize that the same relation holds for the transition to the $F0_u^+(^3P_0)$ state from the mixing intermediate states of ΔJ = odd.

On the contrary, in case (a) which shows the coupling between the rotational states with $\Delta J = 0$, the $B^3\Pi(0_u^+)$ state are combined with the e sublevel of the $c1_g$ state, from which only the P and R branches occur in the $F0_u^+(^3P_0)$–$c1_g$ transition. This relation can be also applied to the mixing states of ΔJ = even.

On these bases we derived the term values of the $F0_u^+(^3P_0)$ state occurring in the spectra. The term value of intermediate state is accurately known.[17] So we scanned the probe laser by installing an intracavity étalon and measured the transition frequency using its fundamental output with an estimated accuracy of 0.02 cm^{-1}. Table 1 summarizes the results on the $F0_u^+(^3P_0)$ $v = 0$ state observed through the (59-0) band of the $B^3\Pi(0_u^+)$–$X^1\Sigma_g^+$ system, together with those obtained through the (57-0)R_{66} and (58-0)P_{70} pump transitions accidentally identified. In this table, we show the occurrence of a single Q branch in the transition to the $F0_u^+(^3P_0)$ state by marking the pump transitions with symbol (*), and the others have the P and R branches. It is not difficult to identify the rotational quantum numbers of the final $F0_u^+(^3P_0)$ state (J_F) from the term values calculated from the known spectroscopic constants. The deviations from the observed to calculated values (δ) are

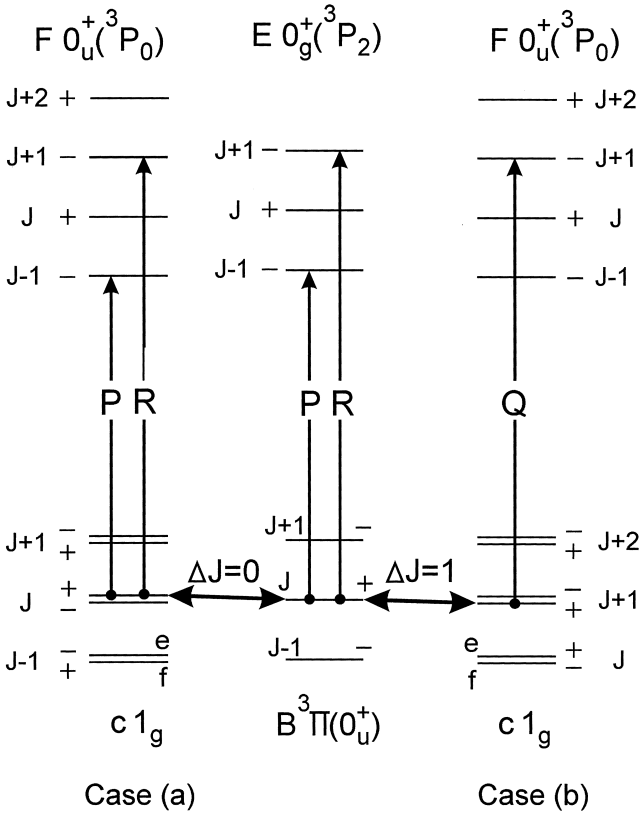

Fig. 2. Coupling schemes between the $B^3\Pi(0_u^+)$ and $c1_g$ valence states. We assumed the rotational quantum number of the intermediate $B^3\Pi(0_u^+)$ state to be even. The selection rules for the rotational transitions from the $B^3\Pi(0_u^+)$–$c1_g$ mixing intermediate state to the $E0_g^+(^3P_2)$ and $F0_u^+(^3P_0)$ ion-pair state are shown. The $F0_u^+(^3P_0)$–$c1_g$ transition has the P and R branches in case (a) where the parity mixing occurs between the states $\Delta J(J_C - J_B) = 0$. It can be applied to the g–u mixing states of ΔJ = even. On the other hand, the $F0_u^+(^3P_0)$–$c1_g$ transition has a single Q branch in case (b) where the parity mixing occurs between the states $\Delta J = 1$. It can be applied to the g–u mixing states of ΔJ = odd.

Table 1. Double Resonance Transitions to the $F0_u^+(^3P_0)$ $v = 0$ State through the Parity Mixing State[a)]

Pump Transition	Frequency / cm^{-1}	T_{vJ}/cm^{-1} Obsd	T_{vJ}/cm^{-1} Calcd[b)]	δ[c)] / cm^{-1}	J_F	Δ_J[d)]
(57-0)R_{66}*	13663.071	47356.026	47356.066	−0.040	66	−1
(58-0)P_{70}	13655.780	47361.547	47361.598	−0.051	68	0
	658.618	367.223	367.292	−0.069	70	
(59-0)R_7	13629.923	47267.195	47267.221	−0.026	9	2
	630.364	268.077	268.083	−0.060	11	
(59-0)P_{21}*	13631.594	47274.865	47274.857	0.008	21	1
(59-0)P_{23}*	13631.973	47276.690	47276.704	−0.014	23	1
(59-0)R_{22}*	13632.182	47277.679	47277.690	−0.021	24	1

a) Pump transitions marked by (*) show a single Q branch to the $F0_u^+(^3P_0)$ state, while the other show the P and R branches.

b) Term values calculated for the J_F rotational level of the $F0_u^+(^3P_0)$ $v = 0$ state.

c) $\delta = T_{vJ}$(obsd) − T_{vJ}(calcd).

d) $\Delta_J = J_c - J_B$.

less than 0.07 cm^{-1}, which is smaller by one order of magnitude than the energy separation between the possible rotational levels of the $F0_u^+(^3P_0)$ states. It is clear that the rotational quantum numbers of the $c1_g$ state defined from the term value analysis are consistent with the results discussed in two types of the coupling schemes between the rotational levels of the $B^3\Pi(0_u^+)$ and $c1_g$ states, ΔJ = even or odd.

In order to find the $B^3\Pi(0_u^+)$–$c1_g$ coupled state further, we switched the final state of the second step of the double resonance from the $F0_u^+(^3P_0)$ state to the $\gamma 1_u(^3P_2)$ and $H1_u(^3P_1)$ states for probing the resonances in the intermediate state. The $\gamma 1_u(^3P_2)$–$c1_g$ and $H1_u(^3P_1)$–$c1_g$ transitions obeying the $\Delta\Omega = 0$ propensity rule are strong enough to detect the other eight resonances, some of which were empirically known and used for probing the $\gamma 1_u(^3P_2)$ state previously. We have analyzed the double resonance spectra consisting of the P and R doublet and elucidated the coupling scheme in the parity mixed intermediate states. The resonances thus found involve the rotational level of the $c1_g$ state up to $J_c = 102$, as listed in Table 2.

2 Analysis of the $2_u(^3P_2)$ Ion-Pair State. A final experiment was performed to identify the $\delta 2_u(^3P_2)$ ion-pair state through the parity mixed $B^3\Pi(0_u^+)$–$c1_g$ intermediate state. Figure 3 shows an example of the double resonance spectrum obtained by pumping the molecules in the $(58\text{-}0)R_{68}$ transition of the $B^3\Pi(0_u^+)$–$X^1\Sigma_g^+$ system. We scanned the probe laser in the 457.6–450.2 nm range while collecting the emission at 342 nm. The $\gamma 1_u(^3P_2)$–$c1_g$ transition is parallel and is composed of the P and R branches with comparable intensity. It is easy to assign this transition from the known spectroscopic constants, as shown in Fig. 3. However, the $\delta 2_u(^3P_2)$–$c1_g$ transition does not obey the $\Delta\Omega = 0$ propensity rule and its transition moment is smaller by one order of magnitude than that of the $\gamma 1_u(^3P_2)$–$c1_g$ system. At the initial stage of experiment, we have a problem to detect the $\delta 2_u(^3P_2)$–$c1_g$ system and must spend time to identify the emission from the $\delta 2_u(^3P_2)$ state to the lower valence state. The $\delta 2_u(^3P_2)$–$c1_g$ transition is perpendicular and is expected to show the P, Q, and R rotational transitions with the 1:2:1 intensity ratio. The transitions actually shows some different spectral features due to the interference effect between the parallel and perpendicular transitions, as discussed later. However, this effect posed no problem in assigning the spectra and we carried out the analysis on the following bases:

(i) The $c1_g$ and $\delta 2_u(^3P_2)$ states are degenerate and are composed of the *e* and *f* sublevels. As shown in Fig. 2, the parity mixing in the intermediate $B^3\Pi(0_u^+)$–$c1_g$ state only occurs in the *e* sublevel of the $c1_g$ state in the case of $\Delta J = 0$ or even, while it occurs in the *f* sublevel in the case of ΔJ = odd. The $\delta 2_u(^3P_2)$–$c1_g$ system allows the *e*–*e* and *f*–*f* transitions in the P and R branches, and the *e*–*f* and *f*–*e* transition in the Q branch. Accordingly, we assigned the $\delta 2_u(^3P_2)$–$c1_g$ transition by following the coupling schemes of the intermediate $B^3\Pi(0_u^+)$–$c1_g$ state catalogued in Tables 1 and 2 and the term values of the $\delta 2_u(^3P_2)$ state were obtained by adding those of the intermediate states.

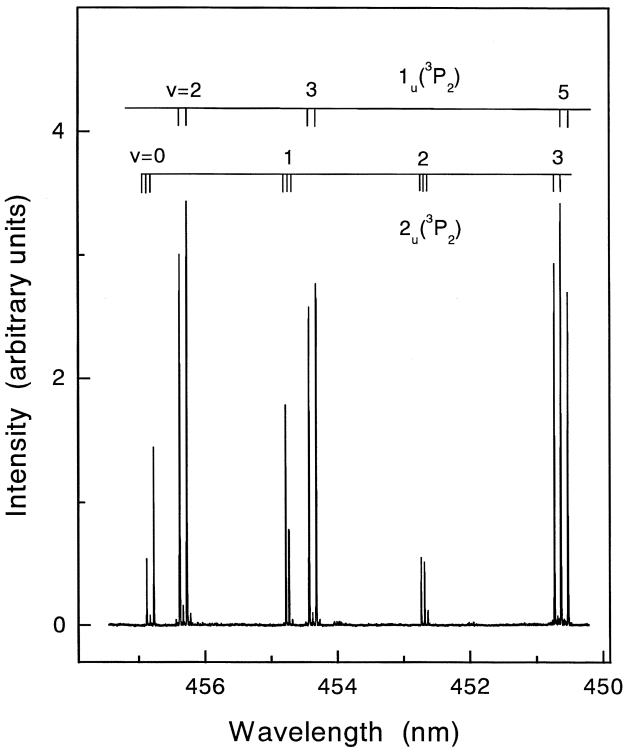

Fig. 3. Double resonance spectrum showing the $\gamma 1_u(^3P_2)$ and $\delta 2_u(^3P_2)$ state. The pump laser excites the $(58\text{-}0)R_{68}$ branch of the $B^3\Pi(0_u^+)$–$X^1\Sigma_g^+$ transition where the $B^3\Pi(0_u^+)$–$c1_g$ mixing occurs. Emission collected at 342 nm.

Table 2. Rotational Lines of the $B^3\Pi(0_u^+)$–$X^1\Sigma_g^+$ Transition Showing the Parity Mixing with the $c1_g$ State

Pump transition	J_c [a]	Δ_J [b]
$(63\text{-}0)P_{104}$	103	0
$(64\text{-}0)R_{97}$	98	0
$(69\text{-}0)R_{57}$	59	1
$(71\text{-}0)R_{59}$	60	0
$(74\text{-}0)R_{41}$	42	0
$(74\text{-}0)R_{42}$	43	0
$(76\text{-}0)R_{42}$	42	−1
$(76\text{-}0)R_{43}$	43	−1

a) Rotational quantum number of the mixed $c1_g$ state.
b) $\Delta_J = J_c - J_B$.

(ii) We have previously detected the $\delta 2_u(^3P_2)$ state by optical–optical double resonance through the $A^3\Pi(1_u)$ state using the (1 + 2) photo-excitation sequence, even though our observation was limited to the levels perturbed by the $\gamma 1_u(^3P_2)$ state.[12] The $\gamma 1_u(^3P_2)$–$\delta 2_u(^3P_2)$ perturbation was then analyzed and the vibrational numbering of the $\delta 2_u(^3P_2)$ state was determined from the magnitude of the perturbation in view of the Franck–Condon overlap between two interacting states. In the present study we dispersed the emission from the $\delta 2_u(^3P_2)$ state: The emission spectrum observed in the first member of the progression at the longer wavelengths shows a single intensity maximum at 342 nm. The second member shows two maxima, indicating the vibrational numbering shown in Fig. 3 in view of the Franck–Condon factors from the ion-pair state to the valence state having shallow potential minimum. The result is of course consistent with the previous vibrational numbering of the $\delta 2_u(^3P_2)$ state. We can assign the emission as terminating on the 2_g state which correlates with the lowest

Table 3. Molecular Constants of the $1_u(^3P_2)$ and $2_u(^3P_2)$ State of I_2[a)]

	$1_u(^3P_2)$[b)]	$2_u(^3P_2)$
Y_{00}	41621.436(6)	41787.780(8)
Y_{10}	94.7483(41)	100.6345(32)
Y_{20}	−0.172516(75)	0.21023(32)
Y_{30}	$2.65(40) \times 10^{-4}$	
Y_{01}	0.0195863(13)	0.0185865(19)
Y_{11}	$-2.781(42) \times 10^{-5}$	$-4.522(24) \times 10^{-5}$
Y_{21}	$-4.13(39) \times 10^{-7}$	
Y_{02}	$-2.82(11) \times 10^{-9}$	$-2.69(13) \times 10^{-9}$

a) All in cm^{-1} and σ in paraentheses.
b) For f sublevels, q_v $(= B_v^e - B_v^f) = 9.54(54) \times 10^{-5} + 2.6(12) \times 10^{-8} \cdot (v + 1/2)^2$.

Table 4. Interaction Matrix Elements ($\beta_{v,v}^{\Omega,\Omega+1}$) between the $1_u(^3P_2)$ and $2_u(^3P_2)$ States[a)]

$1_u(^3P_2)$	$2_u(^3P_2)$	Obsd	Calcd[b)]
$v = 2$	$v = 0$	−0.01158(95)	−0.01413
3	1	−0.01902(39)	−0.01881
4	2	−0.01966(28)	−0.01969
5	3	−0.017342(85)	−0.01788
6	4	−0.013769(29)	−0.01429
7	5	−0.009719(12)	−0.00970
8	6	−0.00475[d)]	−0.00475
9	7	−0.00005[d)]	−0.00005
10	8	−0.00429[d)]	−0.00429
11	9	−0.00772[d)]	−0.00772

a) In cm^{-1} and σ in parentheses.
b) Calculated for $J = 1$.

dissociation limit $I_{3/2} + I_{3/2}$.

We have newly observed 118 transitions in the $9 \leq J \leq 103$ range. They span from $v = 0$ to $v = 7$ for the $\delta 2_u(^3P_2)$ state. We analyzed the $\gamma 1_u(^3P_2)$ and $\delta 2_u(^3P_2)$ states, together with the 606 transitions observed through the $A^3\Pi(1_u)$ state previously, using the following Hamiltonian matrix elements. The diagonal parts represent the energies of the $\gamma 1_u(^3P_2)$ and $\delta 2_u(^3P_2)$ states:

$$\begin{aligned}&\langle \Omega, vJ|H|\Omega, vJ\rangle \\ &= \sum_{lm} Y_{lm}(v+\frac{1}{2})^l \{J(J+1)-\Omega^2\}^m \\ &\quad + \chi \cdot q_{lm}(v+\frac{1}{2})^l \{J(J+1)-\Omega^2\}^m,\end{aligned} \tag{2}$$

where χ is a switching parameter which should only be applied to the $\gamma 1_u(^3P_2)$ state for taking account of the Ω-doubling. The value is +1 for e sublevels and 0 for f sublevels.

The off-diagonal elements are

$$\langle \Omega+1, v'J|H|\Omega, vJ\rangle = -\beta_{v,v}^{\Omega,\Omega+1}\{J(J+1)-\Omega(\Omega+1)\}^{1/2}. \tag{3}$$

In calculations, we only took account of the $\gamma 1_u$–$\delta 2_u(^3P_2)$ interactions between the levels in near resonance. In addition to the interaction between the near resonant levels, the heterogeneous interaction matrix elements are also responsible for more distant interactions with other vibrational levels. However, these effects from the remote Ω', v' states to the v-th vibrational levels of the Ω state were neglected in the analysis and absorbed into the rotational constants.

The present analysis method can determine the interaction terms between the $\gamma 1_u$ and $\delta 2_u(^3P_2)$ states from the energy shift of the $\gamma 1_u(^3P_2)$ and $\delta 2_u(^3P_2)$ states. The fitting is excellent in each energy region, and the standard deviation ($0.0221\ cm^{-1}$) is close to our experimental accuracy. Table 3 summarizes the molecular constants thus obtained for the $\gamma 1_u(^3P_2)$ and $\delta 2_u(^3P_2)$ states. Table 4 lists the $\gamma 1_u(^3P_2)$–$\delta 2_u(^3P_2)$ coupling terms. We have greatly improved the molecular constants of the $\delta 2_u(^3P_2)$ state by expanding our observation over a wider range of the vibrational and rotational states.

The parameters for the heterogenous interaction between the ion-pair states were usually estimated in the pure precession approximation:[17]

$$\begin{aligned}\beta_{v,v}^{\Omega,\Omega+1} &= \eta_{\Omega,\Omega+1}^{el} \cdot B_{v,v}^{\Omega,\Omega+1} \\ &= \langle \Omega+1|L_+ + S_+|\Omega\rangle \langle \Omega+1, v'|h/8\pi^2 c\mu r^2|\Omega, v\rangle,\end{aligned} \tag{4}$$

where $\eta_{\Omega,\Omega+1}^{el} = \{J_a(J_a+1) - \Omega(\Omega+1)\}^{1/2} = 2$. The value of J_a denotes the total angular momentum of the I^+ ion in a separated atom basis set, $|I^+(^3P_J)m_j\rangle|I^-(^1S)m_j\rangle$ representing the wavefunction of the ion-pair state; $J_a = 2$ and $\Omega = 1$ for the $1_u(^3P_2)$–$2_u(^3P_2)$ interaction. The $B_{v,v}^{\Omega,\Omega+1}$ factors can be numerically calculated from the RKR potential curves constructed by the molecular constants in Table 3. Table 4 summarizes the results of these calculations, which are in good agreement with the observed $B_{v,v}^{\Omega,\Omega+1}$ value. This indicates that the pure precession approximation holds for the $1_u(^3P_2)$–$2_u(^3P_2)$ interaction.

3 Intensity Anomaly in the $\delta 2_u(^3P_2)$–$c1_g$ Transition. The spectrum in Fig. 3 shows that the intensity distributions of the $\delta 2_u(^3P_2)$–$c1_g$ transition are anomalous; they do not match the 1:2:1 ratio expected for the P, Q, and R branches of the $\Delta\Omega = +1$ transition. For example, the Q branch in the transition to the $v = 0$ level is quite weak, as expected for the $\Delta\Omega = 0$ transition, and the R branch is twice as strong as the P branch. In increasing v, the Q branch occurs in the $v = 1$ and 2 states, while the P branch grow much bigger than the R branch. Furthermore, apart from the $v = 3$–5 vibrational where the mixing with the $\gamma 1_u(^3P_2)$ state is strong, the rotational transition consists of a Q branch with much stronger R branch in the $v = 6$ and 7 levels of the $\delta 2_u(^3P_2)$ state. A reasonable interpretation on this phenomenon is an interference effect between the parallel and perpendicular transitions.

A heterogeneous interaction is operative between the $\Omega = 1$ and $\Omega = 2$ states. The wavefunction of the $\delta 2_u(^3P_2)$ showing the intensity anomalies consists of the eigen functions of the $2_u(^3P_2)$ and $1_u(^3P_2)$ states, even though the mixing coefficient, C, of the $1_u(^3P_2)$ state is quite small.

$$|\delta 2_u, J\rangle = C\,|1_u, J\rangle + (1 - C^2)^{1/2}|2_u, J\rangle \tag{5}$$

Following the treatment by Lefebvre–Brion and Field, we can derive the approximate relations for the perturbed transition amplitude for larger J states:[18]

$$\begin{aligned}&\{C\mu_\parallel - (1 - C^2)^{1/2}\mu_\perp\}J(J/3)^{1/2} && \text{for R(J)} \\ &(1 - C^2)^{1/2}\mu_\perp J(2J/3)^{1/2} && \text{for Q(J)}\end{aligned}$$

$$\{C\mu_{\parallel} + (1 - C^2)^{1/2}\mu_{\perp}\}J(J/3)^{1/2} \qquad \text{for P(J)},$$

where $\mu_{\parallel}$ and $\mu_{\perp}$ are the transition moments for the parallel $\gamma 1_u(^3P_2)$–$c1_g$ and perpendicular $\delta 2_u(^3P_2)$–$c1_g$ transitions.

It is easy to imagine that the R branch is missing, as seen in the transition to the $\delta 2_u(^3P_2)$ $v = 1$ state, if $C\mu_{\parallel} \sim (1 - C^2)^{1/2}\mu_{\perp}$. If in this case, we can expect that the P branch increases in intensity and becomes twice as large as the Q branch, which is fairly consistent with the intensity distribution in the spectrum. We can evaluate the mixing coefficient (C) from the molecular parameters the $\delta 2_u(^3P_2)$ and $\gamma 1_u(^3P_2)$ states and the perturbation term in Tables 3 and 4. The value of $C = 0.080$ indicates that $(\mu_{\parallel}/\mu_{\perp}) \sim 12.5$.

The R/P intensity anomaly depends on v, since the $\mu_{\parallel}$ and $\mu_{\perp}$ values contains the Franck–Condon overlap between the states involved in the transition. By reference to the molecular constants of the $c1_g$ state reported by Jewsbury et al.,[11] we can predict that the $B^3\Pi(0_u^+)$ ($v_B = 58$, $J_B = 69$) intermediate state is coupled with the $c1_g$ ($v_c = 12$, $J_c = 69$) state. Then the Franck–Condon factors for the $\delta 2_u(^3P_2)$–$c1_g$ and $\gamma 1_u(^3P_2)$–$c1_g$ transitions are calculated. For this purpose, we used the potential function of the $c1_g$ state reported by Jewsbury et al., while we used the RKR potentials for the $\gamma 1_u(^3P_2)$ and $\delta 2_u(^3P_2)$ states constructed by the molecular constants in Table 3. The results reproduces the intensity distribution of vibrational progressions reasonably well. The values of $\langle \gamma 1_u(^3P_2), v = 3|c1_g, v = 12\rangle = 0.126$ and $\langle \delta 2_u(^3P_2), v = 1|c1_g, v = 12\rangle = 0.284$ indicate that the ratio of the electronic transition moments is $(\mu_{\parallel}{}^e/\mu_{\perp}{}^e) \sim 5.5$.

The $\delta 2_u(^3P_2)$ state had not been characterized with reasonable accuracy until recently. A main reason is that the valence to ion-pair states transition obey the $\Delta\Omega = 0$ propensity rule for the transition of the charge transfer property along internuclear axis. Actually our experiments indicated that the $\gamma 1_u(^3P_2)$–$c1_g$ transition is about 30 times stronger than the $\delta 2_u(^3P_2)$–$c1_g$ transition. Perrot et al. reported the ratio of the transition moments for the *gerade* states. The $E0_g^+(^3P_2)$–$B^3\Pi(0_u^+)$ transition is about 30 times stronger than the $\beta 1_g(^3P_2)$–$B^3\Pi(0_u^+)$ transition.[19] They observed the $\beta 1_g(^3P_2)$–$B^3\Pi(0_u^+)$ transition only by the saturation effect of the $E0_g^+(^3P_2)$–$B^3\Pi(0_u^+)$ transition.

In the pioneering works of Danyluk and King, the $\delta 2_u(^3P_2)$ state has been observed as a series of the P/R doublets through the $B^3\Pi(0_u^+)$ state, actually using the *g*–*u* mixed levels.[10] This observation is not surprising. In view of the Franck–Condon factors, the double resonance transitions to the ion-pair state through the parity mixing state occurs as follows: The molecules are first excited to the high vibrational level of the $B^3\Pi(0_u^+)$ state, which couples with the $c1_g$ state by the larger Franck–Condon overlap in the outer turning points of two interacting states. The excitation to the low-vibrational levels of the ion-pair states is achieved from the inner turning points of the $c1_g$ state ($\sim$3.6 Å), which are very close to the potential minimum of the ion-pair states (typically $\sim$3.5 Å). However, the $\delta 2_u(^3P_2)$ state is exceptionally bonded much longer (r_e = 3.78 Å) and the Franck–Condon factors to the lower vibrational states are quite small. The $\delta 2_u(^3P_2)$ state, therefore, occurs in the parallel transition by intensity borrowing from the $\gamma 1_u(^3P_2)$ state, as seen at the $\delta 2_u(^3P_2)$ $v = 0$ state in the spectrum of Fig. 3. This effect is extended to the higher vibrational levels if we use much higher vibrational levels of the intermediate $B^3\Pi(0_u^+)$ state. Further, the $\delta 2_u(^3P_2)$–$\gamma 1_u(^3P_2)$ coupling becomes stronger in the $v = 3$–5 levels of the $\delta 2_u(^3P_2)$ state, due to the presence of the closely-lying $\gamma 1_u(^3P_2)$ state. These vibrational states should have the $\gamma 1_u(^3P_2)$ character in the transition from the $c1_g$ state, showing the P and R branches in the parallel transition.

The authors are grateful for a Hiroshima City University Grant for Special Academic Research (General Studies).

References

1 G. Herzberg, "Spectra of Diatomic Molecules," Van Nostrand, Princeton, NJ (1950).

2 P. R. Bunker and P. Jensen, "Molecular Symmetry and Spectroscopy," NRC Reseach Press, Ottawa (1998).

3 J. P. Pique, F. Hartman, R. Bacis, S. Churassy, and J. B. Koffend, *Phys. Rev. Lett.*, **52**, 267 (1984).

4 J. P. Pique, F. Hatmann, S. Churassy, and R. Bacis, *J. Phys.*, **47**, 1909 (1986).

5 J. C. D. Brand and A. R. Hoy, *Appl. Spectrosc. Rev.*, **23**, 285 (1987).

6 T. Ishiwata, J. Yamada, and K. Obi, *J. Mol. Spectrosc.*, **158**, 237 (1993).

7 T. Ishiwata, H. Takekawa, and K. Obi, *J. Mol. Spectrosc.*, **159**, 443 (1993).

8 T. Ishiwata, T. Kusayanagi, T. Hara, and I. Tanaka, *J. Mol. Spectrosc.*, **119**, 337 (1986).

9 S. Motohiro and T. Ishiwata, *J. Mol. Spectrosc.*, **204**, 286 (2000).

10 M. D. Danyluk and G. W. King, *Chem. Phys.*, **22**, 59 (1977).

11 P. J. Jewsbury, T. Ridley, K. P. Lawley, and R. J. Donovan, *J. Mol. Spectrosc.*, **157**, 33 (1993).

12 T. Ishiwata, S. Motohiro, E. Kagi, H. Fujiwara, and M. Fukushima, *Bull. Chem. Soc. Jpn.*, **73**, 2255 (2000).

13 S. Gersternkorn and P. Luc, "Atlas du spectre d'absortion de la molécule d'iode," CNRS, Paris (1978).

14 S. Gersternkorn, J. Verges, and J. Chevillard, "Atlas du spectre d'absortion de la molécule d'iode," CNRS, Paris (1982).

15 J. Cariou and P. Luc, "Atlas du spectre d'absortion de la molecule de tellure," CNRS, Paris (1998).

16 P. Luc, *J. Mol. Spectrosc.*, **80**, 41 (1980).

17 D. Bassieres and A. R. Hoy, *Can. J. Phys.*, **62**, 1941 (1984).

18 H. Lefebvre-Brion and R. W. Field, "Perturbations in the spectra of diatomic molecules," Academic Press, Orlando, FL (1986).

19 J. P. Perrot, B. Femelat, I. J. Subtil, M. Broyer, and J. Chevaleyre, *Mol. Phys.*, **61**, 97 (1987).